

1 **Initiation mechanisms of enhanced pyrolysis and oxidation of JP-10 (exo-**
2 **tetrahydrodicyclopentadiene) on functionalized graphene sheets: Insights from**
3 **ReaxFF molecular dynamics simulations**

4 Muye Feng^a, Xi Zhuo Jiang^a, Qian Mao^b, Kai H. Luo^{a,*}, Paul Hellier^a

5 ^a *Department of Mechanical Engineering, University College London, Torrington Place, London*
6 *WC1E 7JE, UK*

7 ^b *Department of Energy and Power Engineering, Center for Combustion Energy, Key Laboratory for*
8 *Thermal Science and Power Engineering of Ministry of Education, Tsinghua University, Beijing*
9 *100084, China*

10

11 **Abstract**

12 Functionalized graphene sheets (FGS) have proven to be an effective nanoparticle additive for
13 jet fuels. In this study, the reactive force field (ReaxFF) molecular dynamics (MD) simulation is
14 employed to investigate the initiation mechanisms of JP-10 pyrolysis and oxidation with FGS in
15 comparison with normal JP-10 reactions. ReaxFF-nudged elastic band (NEB) calculations are
16 performed to study the transition state and energy barrier for key initiation reactions in order to
17 reveal the catalytic effect of FGS on JP-10 pyrolysis and oxidation. The results show that both
18 pyrolysis and oxidation of JP-10 are advanced and enhanced in the presence of FGS, leading to
19 earlier decomposition of JP-10 at a lower temperature and a faster reaction rate. It is found that the
20 OH functional group on the FGS not only advances the initiation of JP-10 but also participates in
21 various intermediate reactions to further enhance the pyrolysis and oxidation of JP-10. Moreover, the

* Corresponding author at: Department of Mechanical Engineering, University College London, Torrington Place, London WC1E 7JE, UK. Tel: +44 (0)20 7679 3916. E-mail address: k.luo@ucl.ac.uk (Kai H. Luo)

22 dehydrogenation of JP-10 without FGS is only observed at high temperatures. A deeper insight into
23 the enhancement resulting from the FGS is provided through the analysis of the results of transition
24 state and energy barrier for key initiation reactions. It is found that JP-10 decomposition initiated by
25 OH or H on the FGS occurs at a lower energy barrier than unimolecular decomposition or through
26 reaction with O₂ thereby changing and enhancing the JP-10 initiation. In summary, this research
27 provides the scientific insight as to the potential use of FGS as a promising catalyst for JP-10 fuel
28 systems.

29 **Keywords:** JP-10; Functionalized graphene sheet; Molecular dynamics; Reactive force field;
30 Nudged elastic band calculation; Catalysis.

31 **1. Introduction**

32 Jet Propellant-10 (JP-10, exo-tetrahydrodicyclopentadiene) is a single-component hydrocarbon
33 fuel, which is used in aviation applications such as missiles, detonation engines, ramjets and
34 scramjets due to its extraordinary properties including high energy density [1], high heat capacity [2],
35 high thermal stability [3] and low freezing point [4]. The operational conditions for use of JP-10 as a
36 fuel in pulse-detonation engines can reach up to 2500 K and 100 bar [5]. Because of its broad
37 applications and superior qualities, numerous experimental [2, 6-14] and theoretical [5, 15-21]
38 studies have been reported for the pyrolysis and oxidation of JP-10. However, one problem of JP-10
39 and many other liquid hydrocarbon fuels, is that the slow ignition and combustion kinetics could lead
40 to poor performance for applications like pulse-detonation engines or ramjets [1]. Therefore, research
41 into the catalytic reaction of JP-10 is of theoretical and practical importance. Moreover, the addition
42 of additives can further increase the energy density of the fuel system [22, 23]. Particularly for
43 aeropulsion systems where the cooling requirements are demanding, the catalytic
44 dehydrogenation and cracking of endothermic hydrocarbons like JP-10 is able to offer a better
45 chemical heat sink [24]. To date, the majority of the catalysts used for JP-10 reactions are metal-
46 based materials [1, 24-28] but these suffer from some disadvantages that cannot be ignored. For

47 example, there are non-energetic oxide passivation layers on the particles and undesired solid oxide
48 reaction byproducts produced during the combustion process.

49 In recent years, graphene-based materials, especially functionalized graphene sheets (FGS) have
50 been considered as effective catalysts for fuel and propellant combustion [29-35]. They can not only
51 catalyse fuel combustion reactions, but also be energetically involved in the combustion process, and
52 finally be consumed without producing residual particles. A pioneering work was undertaken by
53 Sabourin et al. [29], who studied the combustion of monopropellant nitromethane enhanced by FGS
54 colloidal particles. They found that the ignition temperature was lowered with the addition of FGS
55 and the burning rate increased up to 175% over neat nitromethane, outperforming more conventional
56 additives such as aluminium oxyhydroxide and amorphous silica oxide nanoparticles. Flame speed
57 enhancement of another monopropellant nitrocellulose by graphene microstructures was also
58 observed in Jain et al.'s [30] experiments. EL-Seesy et al. [31] investigated the impact of adding
59 graphene oxide (GO) nanoparticles to Jatropha Methyl Ester (JME) in a compression ignition (CI)
60 engine and reported that the JME-GO increased the brake thermal efficiency, peak cylinder pressure,
61 highest rate of pressure rise, and peak heat release rate while reducing the duration of combustion
62 and exhaust emissions of CO, UHC and NO_x. Similarly, Paramashivaiah et al. [32] examined the
63 effects of graphene nanoparticles addition to a diesel and biodiesel blend in a CI engine and observed
64 similar effects on engine performance and emission.

65 There has also been increasing interest in using graphene-based materials as additives for jet
66 fuels. Huang and Li [33] explored the ignition and combustion characteristics of jet fuel liquid film
67 containing graphene powders and indicated that the mixture could be ignited with a shorter delay time
68 and that the ignition of graphene occurs prior to that of the jet fuel. Ghamari and Ratner [34] tested
69 the combustion characteristics of colloidal droplets of Jet-A fuel and various carbon-based
70 nanoparticles. Graphene nanoplatelets were found to have an outstanding performance by yielding
71 more than a 7% increase in burning rate at only a 0.1% particle loading. Li et al. [35] recently

72 reported that the application of GO nanosheets on Jet A-1 fuel improved its combustion performance
73 in air in terms of acceleration of initial linear burning velocity, reduction in ignition delay and
74 decrease in strength and speed of initial transmitted wave. Compared with those jet fuels consisting
75 of extremely complex hydrocarbon mixtures, it is certainly of great interest to study the FGS as a
76 promising catalyst for enhancing the reactions of the single-component hydrocarbon fuel JP-10
77 where ignition and combustion kinetics are crucial.

78 To sum up, graphene-based materials are effective catalysts for enhancing fuel and propellant
79 combustion but the understanding of the underlying mechanisms is very limited. Following Sabourin
80 et al.'s [29] pioneering work, Liu et al. [36] studied the enhanced thermal decomposition of
81 nitromethane on FGS by ab initio molecular dynamics (MD) simulations and demonstrated that the
82 catalytic activity originates from the lattice defect complex within the graphene sheet. A reactive
83 force field (ReaxFF) MD simulation research on self-enhanced catalytic activity of FGS in the
84 combustion of nitromethane was completed by Zhang et al. [37]. However, no computational
85 research has been conducted to investigate the potential enhancement by FGS of the reactions of
86 complex hydrocarbons like JP-10 comprising a tricyclic structure. The study of JP-10 as a single-
87 component hydrocarbon fuel is much easier relative to other jet fuels that consist of many hundreds
88 of dissimilar hydrocarbons. In this study, ReaxFF MD simulations are performed to investigate the
89 initiation mechanisms of enhanced pyrolysis and oxidation of JP-10 on FGS and ReaxFF-nudged
90 elastic band (NEB) calculations are conducted to study the transition state and energy barrier for key
91 initiation reactions. Finally, the catalytic effects of FGS on JP-10 pyrolysis and oxidation are
92 revealed.

93 **2. Methodology**

94 ***2.1. Reactive force field (ReaxFF) molecular dynamics (MD) simulation***

95 The ReaxFF MD is a powerful method for modelling dissociation, transition and formation of
96 chemical bonds within a reactive system. In contrast to quantum mechanics (QM)-based methods,

97 ReaxFF features the long-time large-scale reactive MD simulations, which are impractical or
 98 impossible to achieve with QM methods. It is computationally much cheaper than QM methods
 99 while maintaining a high level of accuracy. The concept of bond order is the kernel of ReaxFF and
 100 the force field parameters are obtained from QM calculations or/and experimental data. Bond orders
 101 are calculated directly from interatomic distances (Eq. (1)) and continually updated at every iteration
 102 thereby allowing for connectivity changes [38].

$$\begin{aligned}
 \text{BO}_{ij} &= \text{BO}_{ij}^{\sigma} + \text{BO}_{ij}^{\pi} + \text{BO}_{ij}^{\pi\pi} \\
 &= \exp\left[p_{\text{bo1}}\left(r_{ij}/r_o^{\sigma}\right)^{p_{\text{bo2}}}\right] + \exp\left[p_{\text{bo3}}\left(r_{ij}/r_o^{\pi}\right)^{p_{\text{bo4}}}\right] + \exp\left[p_{\text{bo5}}\left(r_{ij}/r_o^{\pi\pi}\right)^{p_{\text{bo6}}}\right]
 \end{aligned}
 \tag{1}$$

104 where BO is the bond order between atoms i and j , r_{ij} is interatomic distance, r_o terms are
 105 equilibrium bond lengths, and p_{bo} terms are empirical parameters. Equation (1) is continuous for
 106 transitions between σ , π , and $\pi\pi$ bond character, producing a differentiable potential energy surface
 107 as required for calculating the interatomic forces. Equation (2) describes the general energy
 108 contributions to the ReaxFF potential as shown below [39]:

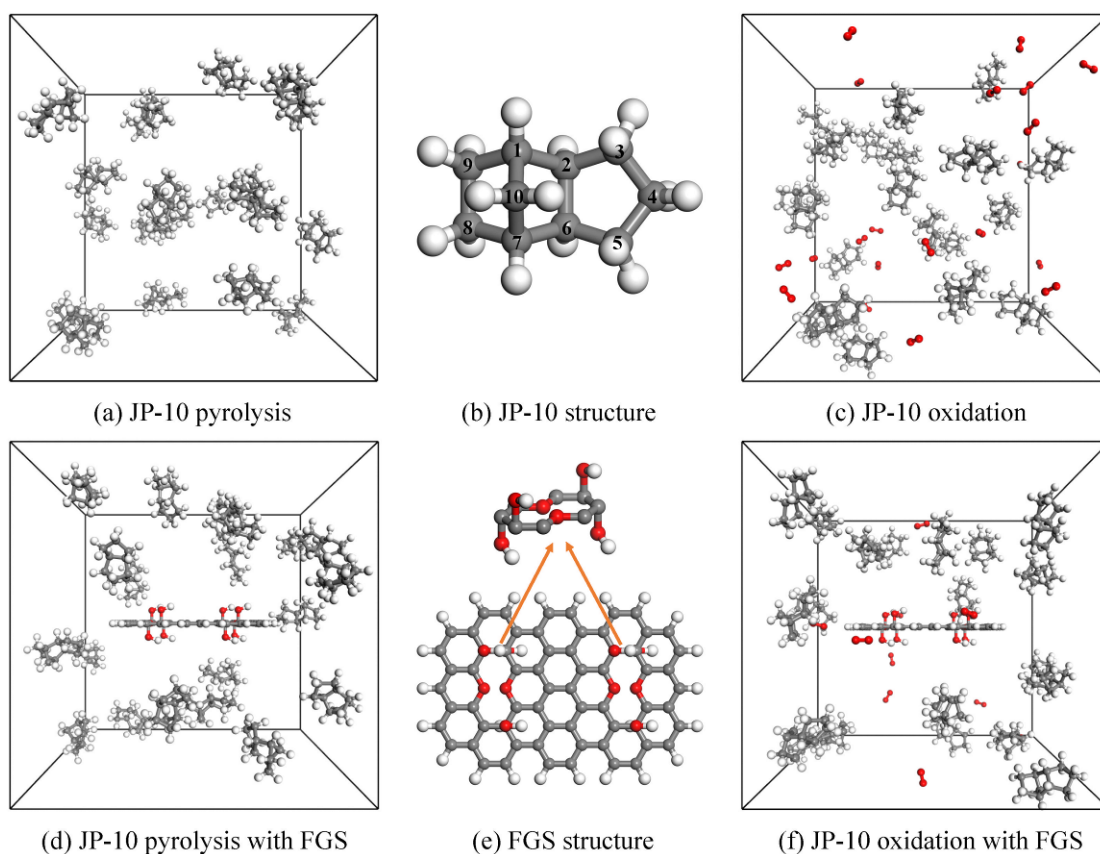
$$E_{\text{system}} = E_{\text{bond}} + E_{\text{over}} + E_{\text{under}} + E_{\text{lp}} + E_{\text{val}} + E_{\text{tor}} + E_{\text{vdWaals}} + E_{\text{Coulomb}}
 \tag{2}$$

110 where E_{system} , E_{bond} , E_{over} , E_{under} , E_{lp} , E_{val} , E_{tor} , E_{vdWaals} and E_{Coulomb} represent total energy, bond
 111 energy, overcoordination energy penalty, undercoordination stability, long pair energy, valence angle
 112 energy, torsion angle energy, van der Waals energy, and Coulomb energy, respectively.

113 Further details of the ReaxFF formulation and development can be found in previous articles [38, 40-
 114 42]. Additionally, ReaxFF MD has proven to be an effective method for studying
 115 hydrocarbon/oxygenated hydrocarbon oxidation with [43-45] or without [39, 46, 47] catalysts.

116 All the ReaxFF MD simulations are performed using the REAXC package embedded in
 117 LAMMPS (Large-scale Atomic/Molecular Massively Parallel Simulator) software [48, 49], with the
 118 latest C/H/O ReaxFF force field parameters [39]. In total, four (pyrolysis and oxidation of JP-10 and

119 their mixture with FGS) three-dimensional and cubic systems with different sizes are established at
120 the same density of 0.15 g/cm^3 . Periodic boundary conditions are applied in all the three directions.
121 Each system contains 20 JP-10 molecules. For the two systems of JP-10 oxidation and its mixture
122 with FGS, 10 oxygen molecules are introduced to focus on the comparison of initiation mechanisms
123 rather than complete oxidation. The details of system construction as well as structure of JP-10 and
124 FGS are shown in Fig. 1. Specifically, the FGS used in this study, which is modified based on a
125 pristine graphene sheet, has 64 carbon, 12 oxygen and 30 hydrogen atoms, and it is placed in the
126 centre of the simulation box. There are 2 identical functional groups on the graphene sheet and each
127 functional group includes a divacancy decorated by 2 ethers with 4 additional OH groups attached to
128 the C atoms nearby [36]. The edge C atoms of the graphene sheet are adjusted with H atoms. To keep
129 the same density, the size of the cubic simulation boxes is accordingly changed for every system and
130 the volume of the FGS is evaluated by creating a Conolly surface with a radius of 1.0 \AA . As a result,
131 the size of all the four systems (Fig. 1a, c, d and f) is 31.11 \AA , 32.29 \AA , 31.38 \AA and 32.53 \AA ,
132 respectively.



133

134 **Fig. 1.** System configurations for pyrolysis and oxidation of JP-10 and their mixture with FGS: (a)
135 JP-10 pyrolysis, (b) JP-10 structure, (c) JP-10 oxidation, (d) JP-10 pyrolysis with FGS, (e) FGS
136 structure and (f) JP-10 oxidation with FGS. C, H and O atoms are represented in grey, white and red,
137 respectively.

138 The canonical ensemble (NVT) is employed for all the ReaxFF MD simulations and the system
139 temperature is controlled by the Nosé-Hoover thermostat with a damping constant of 100 fs. The
140 time step used in this study is 0.1 fs. To start with, energy minimization procedure by conjugate
141 gradient algorithm is carried out for every system to eliminate the artificial effects on the initial
142 geometric configuration. Then the system is equilibrated at the starting temperature 300 K for 50 ps.
143 After the equilibrium, temperature is linearly raised to 2300 K during a time period of 1000 ps
144 (heating rate: 2 K/ps), and finally kept constant at 2300 K for another 1000 ps (heating strategy
145 shown in Fig. 3). Simulation results are outputted every 100 fs. A 0.2 bond order cutoff is adopted
146 for species analysis to recognize the molecules/radicals forming during the simulation because a low
147 cutoff value could benefit the capture of all the reactions including those with very short-lived
148 species [40, 46]. All the visualizations of ReaxFF MD simulation results are produced using Visual
149 Molecular Dynamics (VMD) software [50].

150 **2.2. Nudged elastic band (NEB) calculation**

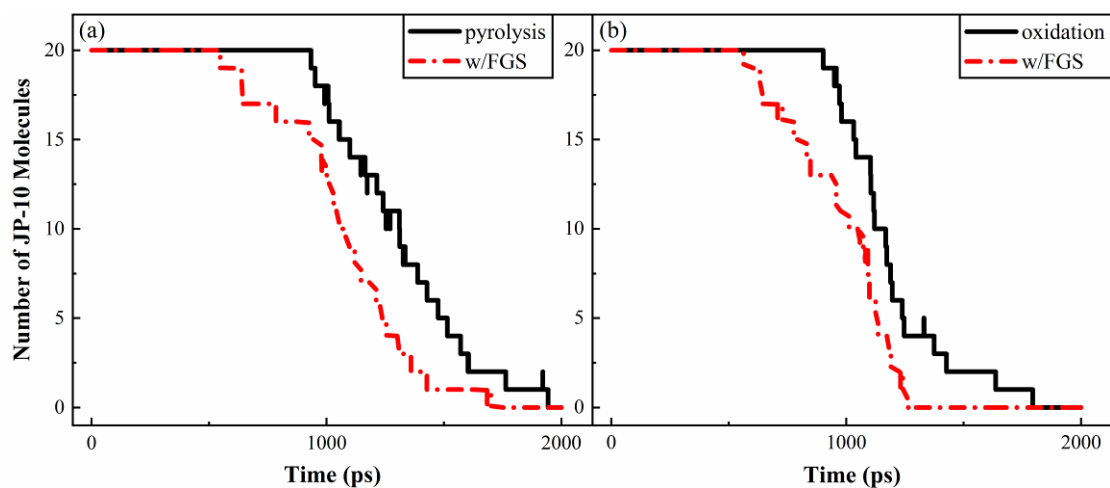
151 Nudged elastic band (NEB) is a method for finding the transition state and calculating the
152 energy barrier of a specific reaction between known reactants and products. A series of intermediate
153 replicas are inserted and the spring force is applied between those replicas in order to find the
154 minimum energy path. The NEB calculation is basically a simultaneous minimization procedure
155 performed via damped dynamics. This method was developed by Henkelman and co-workers [51,
156 52], and has now been widely used in computational chemistry. All the NEB calculations are
157 conducted by the NEB module in LAMMPS. The initial and final structures of all the studied

158 reactions are fully relaxed. Two or three intermediate replicas are generated depending on the
159 complexity of each reaction. The spring constant for connecting each replica is 1 kcal/(mol·Å).

160 **3. Results and discussions**

161 *3.1. Detailed initiation reactions of pyrolysis and oxidation of JP-10 and their mixture with FGS*

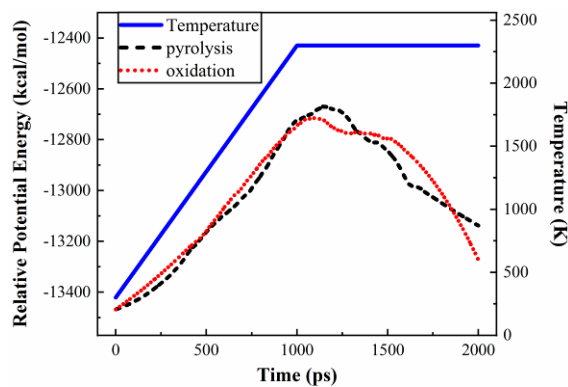
162 The time evolution of the number of JP-10 molecules for all the four systems is shown in Fig. 2.
163 Both pyrolysis and oxidation of JP-10 are enhanced in the presence of FGS, resulting in the earlier
164 decomposition of JP-10 at a lower temperature. Also, the average reaction rate of JP-10 is faster with
165 the addition of FGS in both cases. The enhancement is further confirmed by the change in relative
166 potential energy between JP-10 pyrolysis/oxidation with FGS and JP-10 pyrolysis/oxidation as
167 shown in Fig. 3. These two lines have a similar trend, which increases to a peak firstly and then
168 keeps decreasing. The increase in the difference of relative potential energy means that the heat
169 absorption is accelerated in the systems with FGS. After about 1000 ps, the potential energy of the
170 systems with FGS reaches their peak values and starts to drop down proceeding to the heat release
171 stage but the potential energy of the systems without FGS is still climbing. As a result, the change in
172 relative potential energy subsequently decreases. This also suggests that the reaction of both
173 pyrolysis and oxidation are advanced and enhanced in the presence of FGS. In order to gain deeper
174 insight into the enhancement, the detailed initial decomposition pathway of every single JP-10
175 molecule is tracked by analysing the evolution of species together with the visualization of
176 trajectories. The results are summarized in Tables 1 and 2.



177

178 **Fig. 2.** Time evolution of JP-10 molecule number during NVT MD simulations of: (a) JP-10

179 pyrolysis and its mixture with FGS and (b) JP-10 oxidation and its mixture with FGS.



180

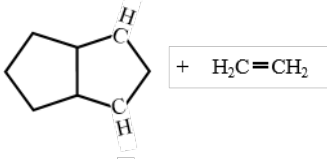
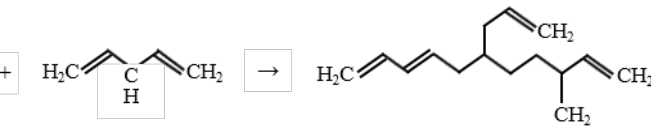
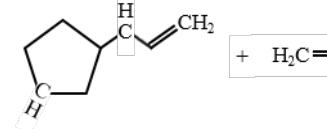
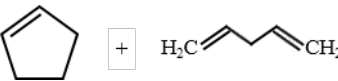
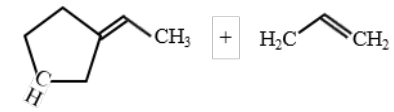
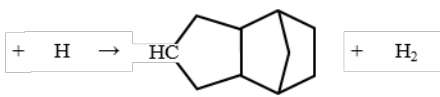
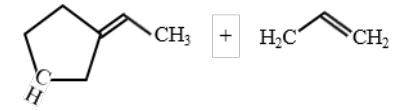
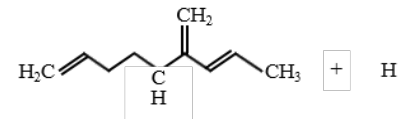
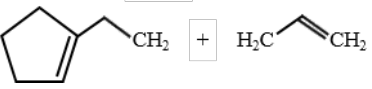
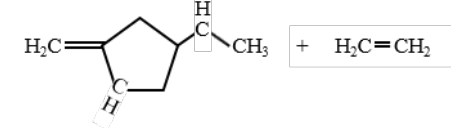
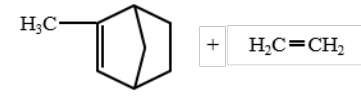
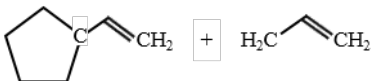
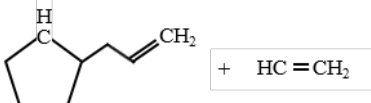
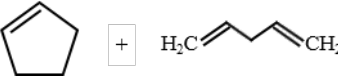
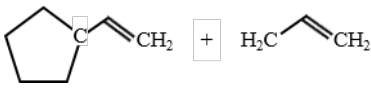
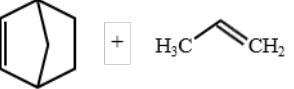
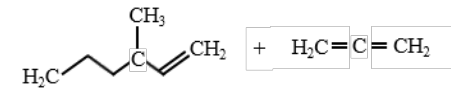
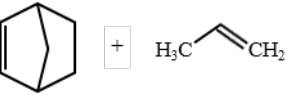
181 **Fig. 3.** Heating strategy and time evolution of relative potential energy between JP-10

182 pyrolysis/oxidation with FGS and JP-10 pyrolysis/oxidation. The noises of two sets of relative

183 potential energy data are reduced by the Savitzky-Golay filter.

184

Table 1. Detailed initial decomposition pathways of every single JP-10 molecule in the systems of: (a) JP-10 pyrolysis and (b) JP-10 pyrolysis with FGS.

No.	(a) Decomposition Reaction	Time (ps)	No.	(a) Decomposition Reaction	Time (ps)
1	 + H ₂ C=CH ₂	934.3	11		1311.9
2	 + H ₂ C=CH ₂	951.9	12		1335.3
3	 + H ₂ C=CH ₂	1007.3	13	 + H ₂	1388.7
4	 + H ₂ C=CH ₂	1011.1	14	 + H	1428.1
5	 + H ₂ C=CH ₂	1056	15		1475.7
6	 + H ₂ C=CH ₂	1099.8	16	 + H ₂ C=CH ₂	1515
7	 + H ₂ C=CH ₂	1164.9	17	 + H	1570.9
8	 + HC≡CH	1214.7	18		1604.9
9	 + H ₂ C=CH ₂	1241.8	19		1763.8
10	 + H ₂ C=CH ₂	1310.4	20		1943.5

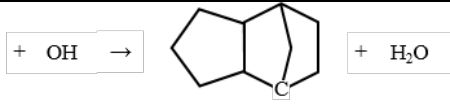
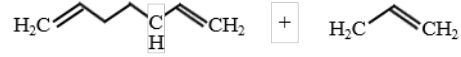
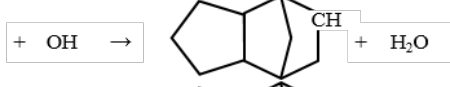
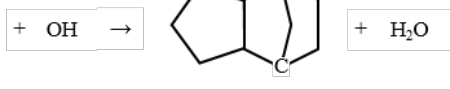
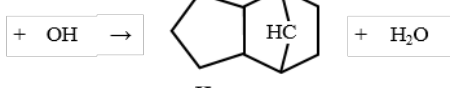
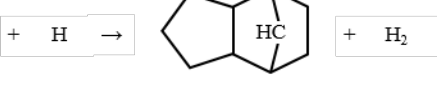
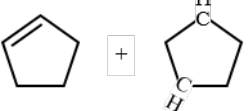
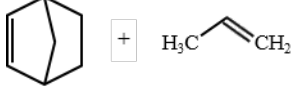
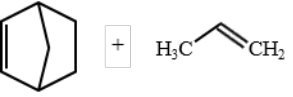
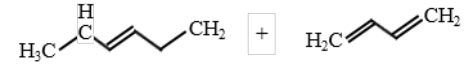
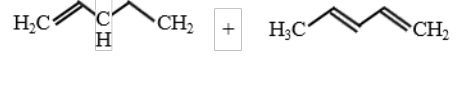
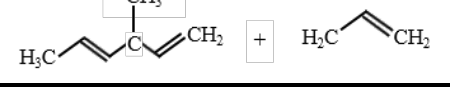
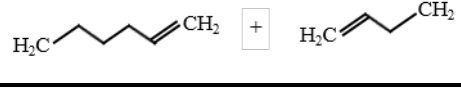
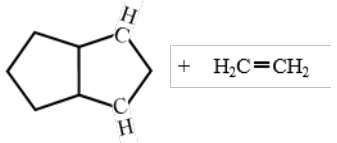
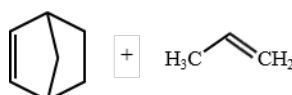
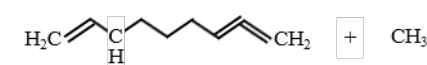
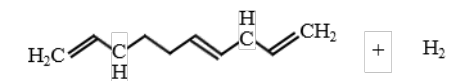
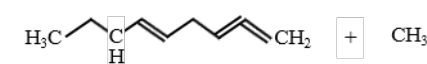
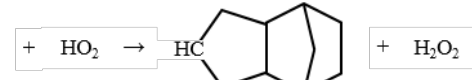
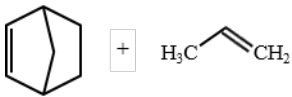
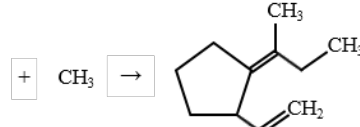
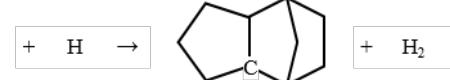
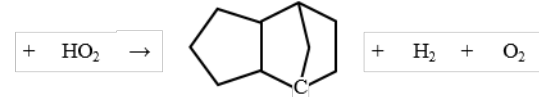
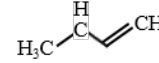
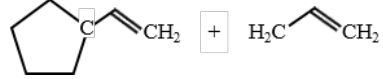
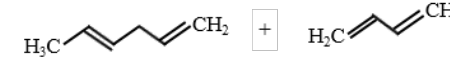
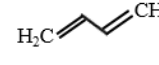
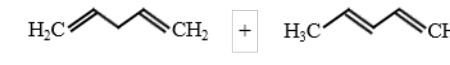
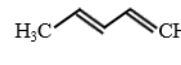
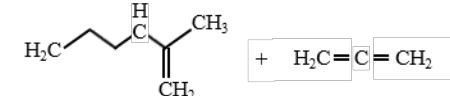
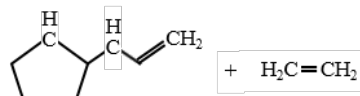
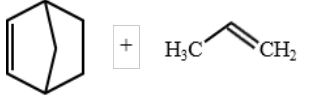
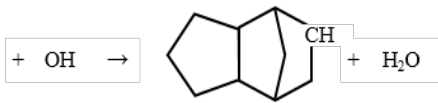
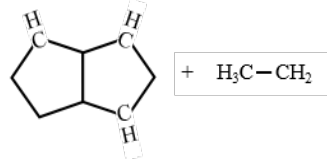
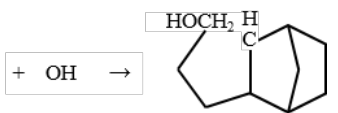
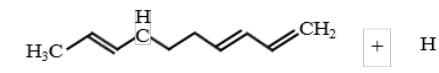
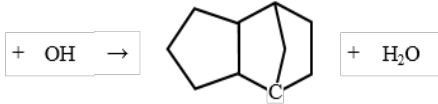
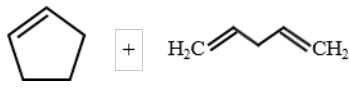
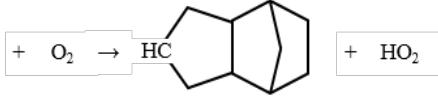
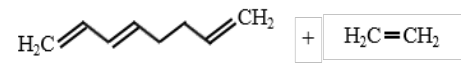
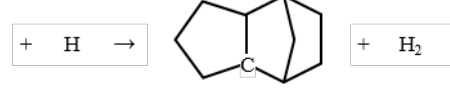
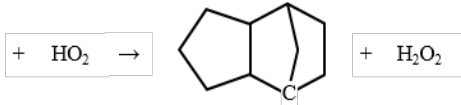
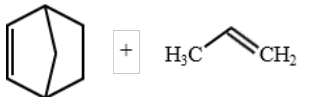
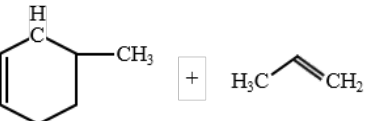
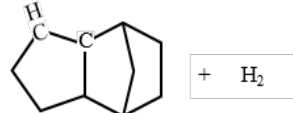
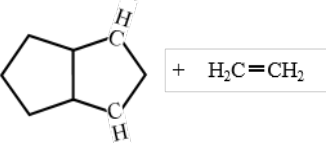
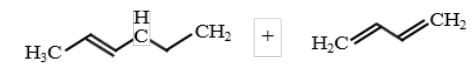
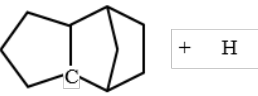
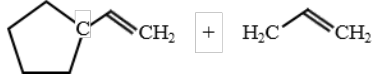
No.	(b) Decomposition Reaction	Time (ps)	No.	(b) Decomposition Reaction	Time (ps)
1		547.7	11		1081.9
2		638.6	12		1120.5
3		642.4	13		1147
4		785.5	14		1211.3
5		925.5	15		1229
6		978.3	16		1255
7		996.5	17		1307.7
8		1011.3	18		1359.5
9		1030.5	19		1427.3
10		1052.9	20		1700.8

Table 2. Detailed initial decomposition pathways of every single JP-10 molecule in the systems of: (a) JP-10 oxidation and (b) JP-10 oxidation with FGS.

No.	(a) Decomposition Reaction	Time (ps)	No.	(a) Decomposition Reaction	Time (ps)
1	 + H ₂ C=CH ₂	902.4	11	 + H ₃ C-CH=CH ₂	1168
2	 + CH ₃	958	12	 + H ₂	1173.5
3	 + CH ₃	971.8	13	+ HO ₂ →  + H ₂ O ₂	1189.2
4	 + H ₃ C-CH=CH ₂	980.5	14	 + H ₂ C=CH ₂	1196.3
5	+ CH ₃ → 	1032.2	15	 + H	1239.1
6	 + H ₂ C-CH=CH-CH=CH ₂	1041.6	16	+ H →  + H ₂	1246.7
7	 + H ₂ C=CH ₂	1104	17	+ HO ₂ →  + H ₂ + O ₂	1375.1
8	 + 	1105.2	18	 + H ₂ C-CH=CH ₂	1427.1
9	 + 	1117.2	19	 + 	1636.9
10	 + H ₂ C=C=CH ₂	1120.6	20	 + H ₂ C=CH ₂	1794.6

No.	(b) Decomposition Reaction	Time (ps)	No.	(b) Decomposition Reaction	Time (ps)
1		563.2	11		1072
2		633.5	12		1092.7
3		643.5	13		1093.6
4		729	14		1099.3
5		777.2	15		1125.3
6		832.2	16		1136
7		848.2	17		1181.8
8		957.4	18		1190.1
9		957.6	19		1241.3
10		1012.1	20		1260.6

184 **3.1.1. Validation of the ReaxFF method**

185 In previous studies, the ReaxFF MD has proven to be an effective method for investigating the
186 pyrolysis and oxidation of JP-10 [46, 53]. Especially, Chenoweth et al. [46] carried out a
187 comprehensive comparison of the JP-10 decomposition products between various experimental [1, 7-
188 9, 54, 55] and their ReaxFF MD results, where a high similarity was found. Among those many
189 decomposition products discovered in experiments, only a couple of them such as C_2H_6 and $C_{10}H_8$
190 (naphthalene) are not observed in the present research. Both Chenoweth et al.'s [46] and this study
191 capture some decomposition products like C_3H_5 (allyl radical) and C_5H_8 (1,4-pentadiene), which
192 were not found in those experiments, but were obtained in several recent experimental studies [6, 12,
193 14]. In addition to the comparison with experimental results, Chenoweth et al. [46] also validated the
194 ReaxFF method by performing QM calculations and the results were in good agreement with each
195 other. Moreover, the latest C/H/O ReaxFF force field parameters used in the present study have
196 proven to be able to produce comparable results of decomposition pathways and Arrhenius
197 parameters for JP-10 as in experiments [39]. Detailed uncertainty analysis including comprehensive
198 and extensive comparison between QM/experimental and ReaxFF data included in the ReaxFF
199 training set, and validation of the quality of the present ReaxFF force field for studying the JP-10
200 chemistry are provided in Ref. [39]. Therefore, it is appropriate to investigate the chemistry of JP-10
201 pyrolysis and oxidation using the ReaxFF MD method with the latest C/H/O parameters.

202 **3.1.2. Effects of FGS addition on JP-10 pyrolysis**

203 The initial step of decomposition for every single JP-10 molecule in the systems of JP-10
204 pyrolysis and its mixture with FGS is presented in Table 1 and the corresponding time of occurrence
205 is given. The JP-10 pyrolysis has been well studied by both experiment [12-14] and numerical
206 modelling [17, 19, 20, 46] before, so this section focuses on the analysis of effects of FGS addition
207 on the JP-10 pyrolysis. In consistency with Ashraf and van Duin's [39] results, for normal pyrolysis,
208 the JP-10 molecules mainly decompose into various smaller hydrocarbons by some dominant

209 pathways (i.e. C₈ & C₂, C₅ & C₅, C₇ & C₃ or C₁₀H₁₅ & H), whereas with FGS, the decomposition of
 210 the first 4 JP-10 molecules begins with the dehydrogenation by the OH group on FGS forming H₂O
 211 and the initiation of these 4 JP-10 molecules all occurs earlier than the first JP-10 decomposition
 212 without FGS. After the initial dehydrogenation, it is also found that the secondary decomposition
 213 into smaller hydrocarbons of these 4 C₁₀H₁₅ radicals happens at 883.8 ps, 893.4 ps, 959.6 ps and 995
 214 ps, respectively, which is more efficient than those JP-10 molecules in normal pyrolysis reactions.
 215 Additionally, the dehydrogenation of JP-10 without FGS (R13, R14 and R17 in Table 1a) is only
 216 observed at a high temperature (2300 K), which also agrees well with the previous results [39].

217 There are in total 8 OH functional groups on the FGS. The results show that 6 of them are
 218 consumed and the remaining 2 are retained at the end of the simulation. Hence, further to the first 4
 219 OH groups, the complete reactions of the 5th and 6th OH group during the whole simulation time are
 220 analysed as well and they are summarized in Table 3. As can be seen, the two series of reactions both
 221 start from the separation of OH from the FGS. Then the OH quickly reacts with a hydrocarbon
 222 radical forming an oxygenated hydrocarbon. Subsequently, the oxygenated hydrocarbon either reacts
 223 with another hydrocarbon or directly decomposes to produce a smaller oxygenated hydrocarbon.
 224 Next, this smaller oxygenated hydrocarbon goes through various reactions or decompositions
 225 generating H₂O or CO eventually. It can be expected that the last 2 OH groups could also take part in
 226 similar intermediate reactions to enhance the pyrolysis reaction, provided that the simulation time is
 227 long enough.

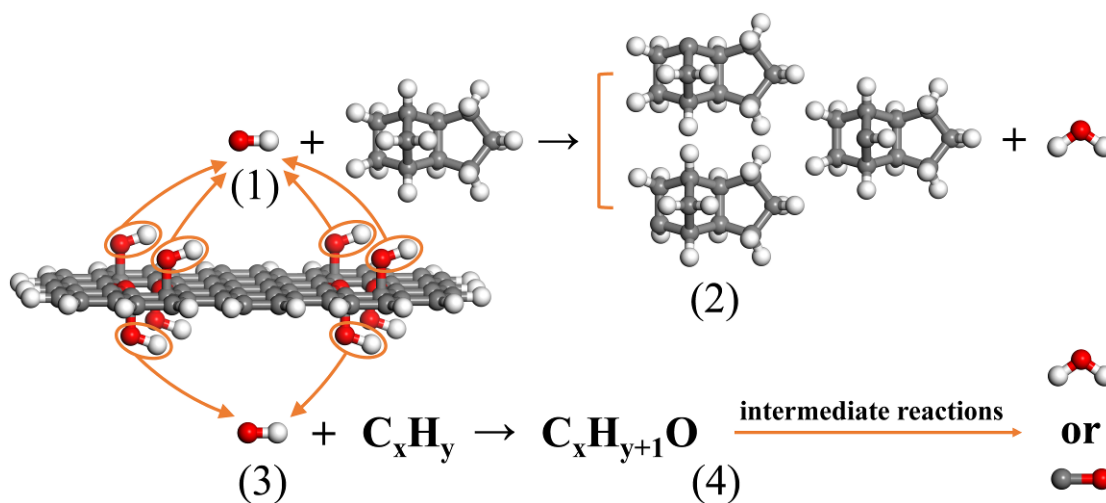
228 **Table 3.** Complete reactions of the 5th and 6th OH group during the whole simulation time of JP-10
 229 pyrolysis with FGS.

Sequence	Time (ps)	Reaction
No. 5 OH		
1	1631.5	OH leaves the FGS
2	1637.9	OH + C ₅ H ₅ → C ₅ H ₆ O
3	1771	C ₅ H ₆ O + C ₇ H ₁₂ → C ₁₀ H ₁₅ + C ₂ H ₃ O
4	1916.1	C ₂ H ₃ O → C ₂ H ₂ + OH

5	1917.7	$\text{OH} + \text{C}_5\text{H}_8 \rightarrow \text{C}_5\text{H}_7 + \text{H}_2\text{O}$
No. 6 OH		
1	1947.3	OH leaves the FGS
2	1947.8	$\text{OH} + \text{C}_6\text{H}_{10} \rightarrow \text{C}_6\text{H}_{11}\text{O}$
3	1954.7	$\text{C}_6\text{H}_{11}\text{O} \rightarrow \text{C}_4\text{H}_7 + \text{C}_2\text{H}_4\text{O}$
4	1967.7	$\text{H} + \text{C}_2\text{H}_4\text{O} \rightarrow \text{H}_2 + \text{C}_2\text{H}_3\text{O}$
5	1976.2	$\text{C}_2\text{H}_3\text{O} \rightarrow \text{C}_2\text{H}_3 + \text{CO}$

230

231 Combing the above two paragraphs, the catalytic reaction steps for JP-10 pyrolysis on FGS can
 232 be summarized as follow (Fig. 4): (1) OHs leave the FGS; (2) OHs initiate the pyrolysis reaction by
 233 reacting with JP-10 forming $\text{C}_{10}\text{H}_{15}$ and H_2O ; (3) more OHs leave the FGS; (4) OHs take part in
 234 various intermediate reactions involving oxygenated hydrocarbons. It is indicated that the OH
 235 functional groups on the FGS can not only advance the initiation of JP-10 pyrolysis, but also
 236 participate in various intermediate reactions to further enhance the pyrolysis reaction.



237

238 **Fig. 4.** Catalytic reaction steps for JP-10 pyrolysis on FGS: (1) OHs leave the FGS; (2) OHs initiate
 239 the pyrolysis reaction by reacting with JP-10 forming $\text{C}_{10}\text{H}_{15}$ and H_2O ; (3) more OHs leave the FGS;
 240 (4) OHs take part in various intermediate reactions involving oxygenated hydrocarbons.

241 3.1.3. Effects of FGS addition on JP-10 oxidation

242 Table 2 presents the initial decomposition step for every single JP-10 molecule and its
 243 corresponding time of occurrence in the systems of JP-10 oxidation and its mixture with FGS. The

244 analysis of effects of FGS addition rather than the simple JP-10 oxidation is emphasized in this
 245 section. The results show that the initiation of normal JP-10 oxidation includes two main stages, i.e.
 246 (1) decomposition of JP-10 and (2) reaction of JP-10 and other decomposed products with radicals
 247 like O₂, O, H, OH, HO₂ and H₂O₂, which is in accordance with previous experimental [6] and
 248 computational [5, 53] results. In contrast to JP-10 pyrolysis with FGS, the pathways are different
 249 although the decomposition of the first 4 JP-10 molecules in the system of JP-10 oxidation with FGS
 250 is still initiated by the reaction with OH. A new pathway is found, which involves the C-C bond
 251 cleavage followed by OH attachment to one of those two C atoms (R1 and R3 in Table 2b). The
 252 complete reactions that these two C₁₀H₁₆OH molecules undergo during the simulation time are listed
 253 in Table 4. They both firstly decompose into a smaller oxygenated hydrocarbon and then this
 254 oxygenated hydrocarbon goes through a series of reactions to finally form CO and H₂O, respectively.
 255 It is worth noting that a short exchange between intermediate products and FGS (R3 and R4 in Table
 256 4 – No. 2 C₁₀H₁₆OH) is observed in the reactions of the second C₁₀H₁₆OH molecule. The same as JP-
 257 10 pyrolysis reactions, the initiation of the first 4 JP-10 molecules in the system of JP-10 oxidation
 258 with FGS all proceed earlier than the first JP-10 decomposition without FGS and the
 259 dehydrogenation of JP-10 without FGS (R12, R13, R15, R16 and R17 in Table 2a) only takes place
 260 at a high temperature (2300 K).

261 **Table 4.** Complete reactions of two C₁₀H₁₆OH molecules during the whole simulation time of JP-10
 262 oxidation with FGS. The subscript of FGS represents the different forms of FGS containing different
 263 numbers of C, H and/or O atoms.

No. 1 C ₁₀ H ₁₆ OH (1 st JP-10 molecule)		
Sequence	Time (ps)	Reaction
1	674.2	C ₁₀ H ₁₇ O → C ₂ H ₅ O + C ₈ H ₁₂
2	961	OH + C ₂ H ₅ O → C ₂ H ₆ O ₂
3	1196.2	C ₂ H ₆ O ₂ → CH ₃ + CH ₃ O ₂
4	1328.2	H + CH ₃ O ₂ → H ₂ + CH ₂ O ₂
5	1594.9	H + CH ₂ O ₂ → CH ₃ O ₂
6	1595.2	CH ₃ O ₂ → H ₂ O + CHO

7	1597.7	$C_2H_3 + CHO \rightarrow C_3H_4O$
8	1598.4	$C_3H_4O \rightarrow H + C_3H_3O$
9	1616.2	$C_3H_3O \rightarrow C_2H_3 + CO$
No. 2 C₁₀H₁₆OH (3rd JP-10 molecule)		
Sequence	Time (ps)	Reaction
1	1063.3	$C_{10}H_{17}O \rightarrow C_9H_{14}O + CH_3$
2	1117.2	$C_9H_{14}O \rightarrow C_6H_{10}O + C_3H_4$
3	1123.1	$C_6H_{10}O + FGS_1 \rightarrow FGS_2$
4	1124.7	$FGS_2 + C_{10}H_{14} \rightarrow FGS_1 + C_6H_{10}O + C_2H_4 + C_8H_{10}$
5	1353	$H + C_6H_{10}O \rightarrow C_6H_{11}O$
6	1353.1	$C_6H_{11}O \rightarrow C_6H_9 + H_2O$

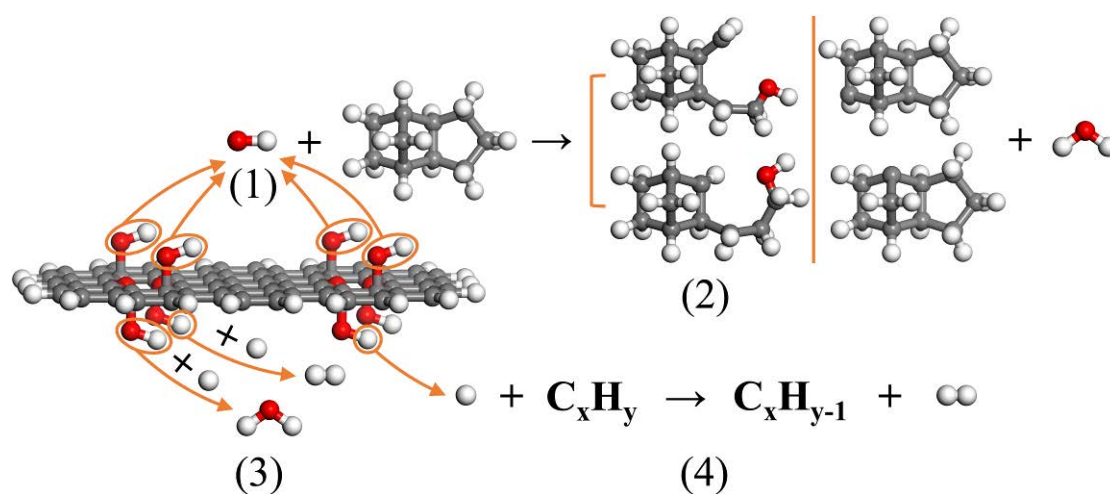
264 With respect to the 8 OH functional groups on the FGS, 6 of them are consumed, leaving 1 OH
265 group and 1 attached O (lose the H) at the end of the simulation. The complete reactions of the 5th,
266 6th and 7th OH groups during the simulation time are shown in Table 5. Unlike those OHs in
267 pyrolysis reactions which react with hydrocarbon intermediates, the 5th and 6th OH groups are
268 attracted by an H radical directly generating H₂O and H₂, respectively, while the H is found to detach
269 from the 7th OH and then dehydrogenize a hydrocarbon producing H₂. This difference results from
270 the introduction of O₂ generating more OHs from HO₂ and H₂O₂ as well as some oxygenated
271 hydrocarbons which both react with hydrocarbon radicals. Besides, the O₂ itself can also compete
272 with OH's reaction with hydrocarbons. Due to these reasons, O-H bond cleavage of the OH group on
273 the FGS is only observed in the oxidation reactions. In addition, the H of OH can transfer between
274 different O atoms on the FGS. For example, at 1228.4 ps, an H of OH moves to a nearby O of ether
275 and transfers back to the original O of that OH later at 1512.6 ps. Similarly, in the two reactions of
276 No. 6 OH in Table 5, after losing the H, the O of OH shifts to another edge C atom of FGS and
277 finally leaves the FGS as CO. The remaining one OH group and one attached O could also be
278 involved in the intermediate reactions to further accelerate the JP-10 oxidation if the simulation is
279 continued.

280 **Table 5.** Complete reactions of the 5th, 6th and 7th OH groups during the whole simulation time of JP-
 281 10 oxidation with FGS. All reactions involving FGS relate to the OH group on it. The subscript of
 282 FGS represents the different forms of FGS containing different numbers of C, H and/or O atoms.

Sequence	Time (ps)	Reaction
No. 5 OH		
1	1018.7	$\text{H} + \text{FGS}_1 \rightarrow \text{FGS}_2$
2	1018.8	$\text{FGS}_2 \rightarrow \text{FGS}_3 + \text{H}_2\text{O}$
No. 6 OH		
1	1030.5	$\text{H} + \text{FGS}_3 \rightarrow \text{FGS}_4 + \text{H}_2$
2	1986.6	CO leaves the FGS
No. 7 OH		
1	1755.3	$\text{FGS}_5 \rightarrow \text{FGS}_6 + \text{H}$
2	1759	$\text{H} + \text{C}_8\text{H}_{10} \rightarrow \text{C}_8\text{H}_9 + \text{H}_2$

283

284 To summarize, the catalytic reaction steps for JP-10 oxidation on FGS follow the procedure
 285 (Fig. 5): (1) OHs leave the FGS; (2) OHs initiate the oxidation reaction by reacting with JP-10 via
 286 different pathways; (3) OH or H of OH is abstracted from or leaves the FGS; (4) OH or H take part
 287 in intermediate reactions involving the direct formation of H₂O and H₂. Again, it is the OH
 288 functional group that advances the initiation of JP-10 oxidation and further enhances the oxidation
 289 reaction by participating in various intermediate reactions.

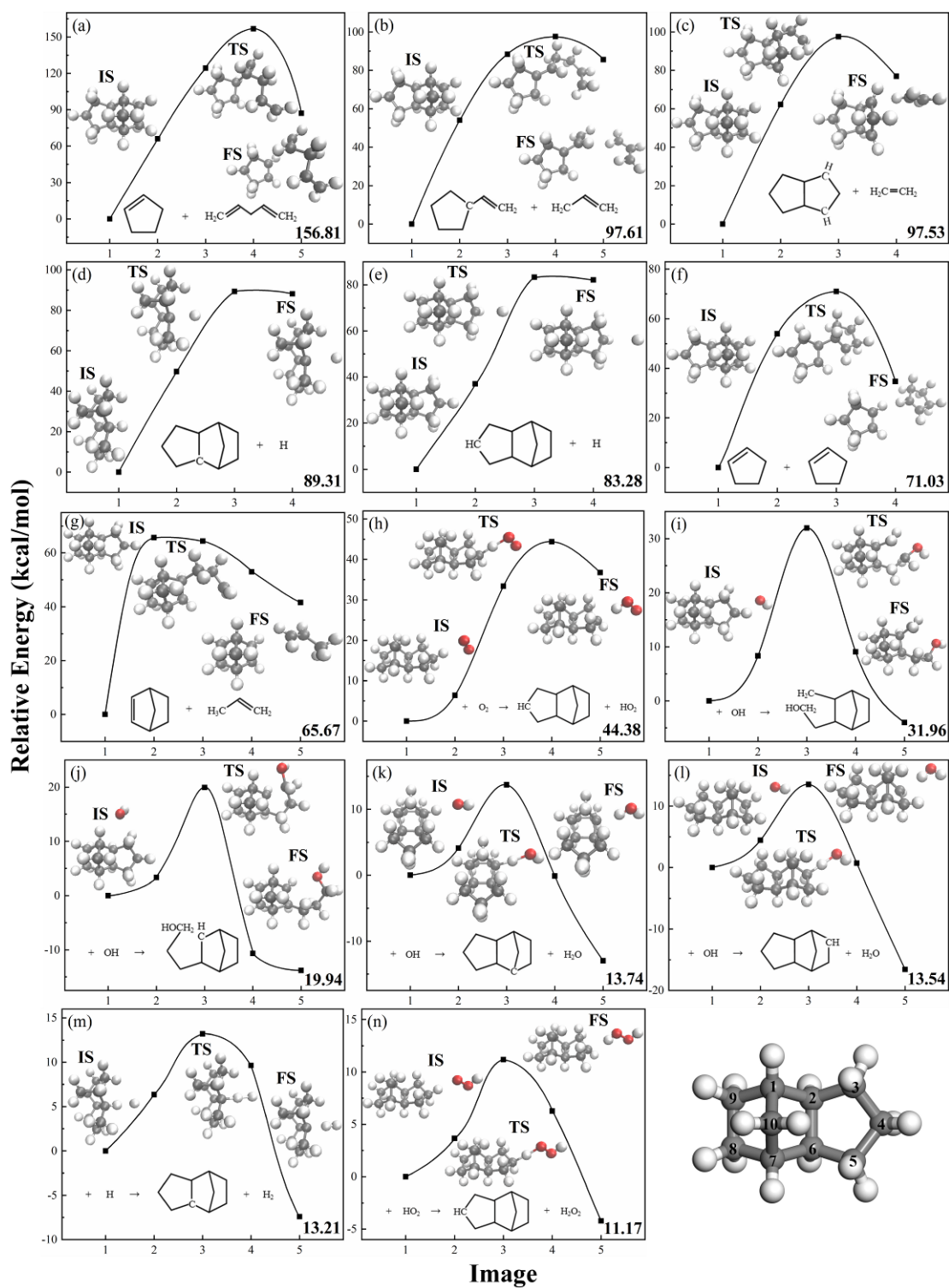


290

291 **Fig. 5.** Catalytic reaction steps for JP-10 oxidation on FGS: (1) OHs leave the FGS; (2) OHs initiate
 292 the oxidation reaction by reacting with JP-10 via different pathways; (3) OH or H of OH is abstracted

293 from or leaves the FGS; (4) OH or H take part in intermediate reactions involving the direct
 294 formation of H₂O and H₂.

295 **3.2. Transition state and energy barrier for key initiation reactions**



296

297 **Fig. 6.** Transition state and energy barrier for some frequently occurring and key JP-10

298 decomposition reactions from ReaxFF-NEB simulations. Figs. a–f are placed in the descending order

299 of energy barrier and the calculated value of energy barrier is labelled in the bottom right corner in
300 each figure. The C atoms of JP-10 molecule are numbered in the last figure.

301 Fig. 6 depicts the transition state and energy barrier for some frequently occurring and key JP-
302 10 decomposition reactions extracted from Tables 1 & 2 by ReaxFF-NEB simulations. It is checked
303 that all of the obtained transition states from NEB calculations accord with the dynamic trajectories
304 of ReaxFF MD simulations. Among all these studied reactions, the decomposition of JP-10 to
305 cyclopentene and 1,4-pentadiene (Fig. 6a) has the highest energy barrier of 156.81 kcal/mol. This
306 decomposition procedure follows the sequential cleavage of C-C bonds: $C_8-C_9 \rightarrow C_1-C_2 \rightarrow C_6-C_7$,
307 which is the same as Chenoweth et al.'s results [46]. The sequence of C-C bond dissociation for the
308 reaction producing allyl in Fig. 6b is $C_1-C_2 \rightarrow C_7-C_{10} \rightarrow C_8-C_9$ and the H attached to C_6 shifts to C_2
309 before the cleavage of C_7-C_{10} bond. These reaction steps are also found in DFT calculations [20].
310 Fig. 6c demonstrates the formation of ethylene resulting from the successive breaking of C-C bonds
311 between C_1 & C_9 and C_7 and C_8 . The C_2-C_6 bond broken is seen at a later stage of the simulation
312 leading to 1,5-cyclooctadiene structure. The JP-10 decomposition products of 1,5-cyclooctadiene and
313 ethylene agree with the DFT [18] and ReaxFF MD [46] simulation results. These two reactions in
314 Figs. 6b & c have very close energy barrier values. Figs. 6d & e illustrate the two scenarios of
315 dehydrogenation of JP-10 at C_2 and C_4 , respectively. Zhao et al. [14] computed the energy of C-H
316 bond cleavage for every C position of JP-10 by DFT and found that the dehydrogenation at C_2 , C_3 ,
317 C_4 and C_9 are more preferable with the energy ranging from 92.73–97.04 kcal/mol. Three (C_2 , C_3 and
318 C_4) of these four dehydrogenations are observed in the present study and the calculated energy
319 barrier for dehydrogenation at C_2 (89.31 kcal/mol) and C_4 (83.28 kcal/mol) is in good agreement with
320 Zhao et al.'s DFT calculations. The conversion of JP-10 to two five-member ring structures were
321 discovered in many studies [6, 7, 12, 14, 17]. The C_1-C_2 bond is broken first followed by further
322 fragmentation via C_6-C_7 separation. In this study (Fig. 6f), before the C_6 is separated from C_7 , one H
323 attached to C_{10} moves to C_1 producing two cyclopentenes eventually. Fig. 6g describes the formation

324 of 2-norbornene and propene from consecutive C₅-C₆ and C₂-C₃ bond scissions [6, 7, 17, 19], which
325 also involves the H transfer from C₄ to C₅ prior to the cleavage of C₂-C₃ bond.

326 Other species, i.e. O₂, OH, H and HO₂ are introduced in the JP-10 initiation reactions in Figs.
327 6h–n and the energy barriers of these reactions are all lower than the above unimolecular JP-10
328 decompositions as expected. Except for the two reactions in Figs. 6i & j, the remaining five all relate
329 to the dehydrogenation of JP-10 at various C positions. It can be seen that the dehydrogenation of JP-
330 10 by O₂ has the highest energy barrier of 44.38 kcal/mol among these reactions, followed by the
331 formation of two C₁₀H₁₆OHs with OH attaching to C₄ and C₃, respectively. The OH is more likely to
332 attach to C₃ compared to C₄ because the energy barrier is much lower. Figs. 6k & l show the
333 dehydrogenation of JP-10 by the OH functional group on FGS at C₁ and C₈ producing H₂O and the
334 energy barriers for these two reactions are almost the same. It is indicated that JP-10 decomposition
335 initiated by OH is easier than by O₂. The H₂ formation via dehydrogenation of JP-10 by the H radical
336 in Fig. 6m has a similar energy barrier as those decompositions initiated by OH. As presented in
337 Table 5, the FGS can release the H of OH to participate in intermediate reactions, which could also
338 be helpful for JP-10 initiation. It can be expected to see the JP-10 reaction with H of OH on FGS if
339 the size of FGS is increased with more OH functional groups. The energy barrier of the
340 dehydrogenation of JP-10 by HO₂ generating H₂O₂ is slightly lower than those reactions in Figs. 6k–
341 m. However, it needs HO₂ as a precursor and the formation of HO₂ is not that straightforward and
342 easy as the release of OH or H from FGS. Based on the above analysis, it can be concluded that the
343 energy barrier for JP-10 decomposition reactions initiated by the OH or potential H of OH on FGS is
344 much lower than the unimolecular decomposition of JP-10 by the C-C or C-H bond scission. This
345 considerable reduction in the energy barrier makes the reactions of JP-10 with OH or H on FGS more
346 preferable than those cleavages of C-C or C-H bonds thereby changing and enhancing the JP-10
347 initiation.

348 **4. Conclusions**

349 The ReaxFF MD simulations are performed to investigate the initiation mechanisms of JP-10
350 pyrolysis and oxidation with FGS in comparison with normal JP-10 reactions. Moreover, the
351 ReaxFF-NEB calculations are conducted to study the transition state and energy barrier for some key
352 initiation reactions. The results show that both pyrolysis and oxidation of JP-10 are advanced and
353 enhanced in the presence of FGS, leading to earlier decomposition of JP-10 at a lower temperature
354 and a faster reaction rate. The detailed initiation reactions of pyrolysis and oxidation of JP-10 and
355 their mixture with FGS are obtained to scrutinize the effect of FGS addition. Compared with
356 pyrolysis of pure JP-10 mainly decomposing to various smaller hydrocarbons, the decomposition of
357 JP-10 with FGS starts with the dehydrogenation by the OH functional groups on the FGS forming
358 H₂O. Similarly, in the system of JP-10 oxidation with FGS, the decomposition of JP-10 is initiated
359 by its reaction with OH. In addition to the H₂O formation, another pathway that involves the C-C
360 bond cleavage followed by OH attachment to one of those two C atoms is observed. For both JP-10
361 pyrolysis and oxidation, as the reaction proceeds, more OH groups of FGS take part in various
362 intermediate reactions involving oxygenated hydrocarbons or direct production of H₂O and H₂ as
363 well. Moreover, the dehydrogenation of JP-10 without FGS only occurs at high temperatures.
364 Therefore, it is the OH functional group on the FGS that not only advances the initiation of JP-10 but
365 also participates in various intermediate reactions to further enhance the pyrolysis and oxidation of
366 JP-10. A deeper insight into the enhancement resulting from the FGS is provided by the results of
367 transition state and energy barrier for key initiation reactions. It is found that the JP-10
368 decomposition initiated by OH or H occurs at a lower energy barrier than unimolecular
369 decomposition or through reaction with O₂. This makes the reactions of JP-10 with OH or H on the
370 FGS preferable thereby changing and enhancing the JP-10 initiation. This research lays the scientific
371 foundation for the potential use of FGS as a promising catalyst for JP-10 fuel systems.

372 **Acknowledgements**

373 Funding from the UK Engineering and Physical Sciences Research Council under the project
374 “UK Consortium on Mesoscale Engineering Sciences (UKCOMES)” (Grant Nos. EP/L00030X/1
375 and EP/R029598/1) is gratefully acknowledged. The first author is also grateful for the Graduate
376 Research Scholarship and Overseas Research Scholarship from University College London.

377 **Declarations of interest:** none

378 **References**

- 379 [1] Van Devener B, Anderson SL. Breakdown and combustion of JP-10 fuel catalyzed by
380 nanoparticulate CeO₂ and Fe₂O₃. *Energ Fuel* 2006;20(5):1886-94.
- 381 [2] Davidson DF, Horning DC, Herbon JT, Hanson RK. Shock tube measurements of jp-10
382 ignition. *P Combust Inst* 2000;28:1687-92.
- 383 [3] Osmont A, Gokalp I, Catoire L. Evaluating missile fuels. *Propell Explos Pyrot*
384 2006;31(5):343-54.
- 385 [4] Edwards T. Advancements in gas turbine fuels from 1943 to 2005. *J Eng Gas Turb Power*
386 2007;129(1):13-20.
- 387 [5] Li SC, Varatharajan B, Williams FA. Chemistry of JP-10 ignition. *Aiaa J* 2001;39(12):2351-
388 6.
- 389 [6] Gao CW, Vandeputte AG, Yee NW, Green WH, Bonomi RE, Magoon GR, et al. JP-10
390 combustion studied with shock tube experiments and modeled with automatic reaction
391 mechanism generation. *Combust Flame* 2015;162(8):3115-29.
- 392 [7] Herbinet O, Sirjean B, Bounaceur R, Fournet R, Battin-Leclerc F, Scacchi G, et al. Primary
393 mechanism of the thermal decomposition of tricyclodecane. *J Phys Chem A*
394 2006;110(39):11298-314.
- 395 [8] Nakra S, Green RJ, Anderson SL. Thermal decomposition of JP-10 studied by micro-
396 flowtube pyrolysis-mass spectrometry. *Combust Flame* 2006;144(4):662-74.

- 397 [9] Rao PN, Kunzru D. Thermal cracking of JP-10: Kinetics and product distribution. *J Anal*
398 *Appl Pyrol* 2006;76(1-2):154-60.
- 399 [10] Seiser R, Niemann U, Seshadri K. Experimental study of combustion of n-decane and JP-10
400 in non-premixed flows. *P Combust Inst* 2011;33:1045-52.
- 401 [11] Striebich RC, Lawrence J. Thermal decomposition of high-energy density materials at high
402 pressure and temperature. *J Anal Appl Pyrol* 2003;70(2):339-52.
- 403 [12] Vandewiele NM, Magoon GR, Van Geem KM, Reyniers MF, Green WH, Marin GB.
404 Experimental and Modeling Study on the Thermal Decomposition of Jet Propellant-10. *Energ*
405 *Fuel* 2014;28(8):4976-85.
- 406 [13] Xing Y, Fang WJ, Xie WJ, Guo YS, Lin RS. Thermal Cracking of JP-10 under Pressure. *Ind*
407 *Eng Chem Res* 2008;47(24):10034-40.
- 408 [14] Zhao L, Yang T, Kaiser RI, Troy TP, Xu B, Ahmed M, et al. A vacuum ultraviolet
409 photoionization study on high-temperature decomposition of JP-10 (exo-
410 tetrahydrodicyclopentadiene). *Phys Chem Chem Phys* 2017;19(24):15780-807.
- 411 [15] Hudzik JM, Asatryan R, Bozzelli JW. Thermochemical Properties of exo-
412 Tricyclo[5.2.1.0(2,6)]decane (JP-10 Jet Fuel) and Derived Tricyclodecyl Radicals. *J Phys*
413 *Chem A* 2010;114(35):9545-53.
- 414 [16] Magoon GR, Aguilera-Iparraguirre J, Green WH, Lutz JJ, Piecuch P, Wong HW, et al.
415 Detailed chemical kinetic modeling of JP-10 (exo-tetrahydrodicyclopentadiene) high-
416 temperature oxidation: Exploring the role of biradical species in initial decomposition steps.
417 *Int J Chem Kinet* 2012;44(3):179-93.
- 418 [17] Morozov AN, Mebel AM, Kaiser RI. A Theoretical Study of Pyrolysis of exo-
419 Tetrahydrodicyclopentadiene and Its Primary and Secondary Unimolecular Decomposition
420 Products. *J Phys Chem A* 2018;122(22):4920-34.

- 421 [18] Qin XM, Xie HJ, Yue L, Lu XX, Fang WJ. A quantum chemistry study on thermochemical
422 properties of high energy-density endothermic hydrocarbon fuel JP-10. *J Mol Model*
423 2014;20(4).
- 424 [19] Vandewiele NM, Magoon GR, Van Geem KM, Reyniers MF, Green WH, Marin GB. Kinetic
425 Modeling of Jet Propellant-10 Pyrolysis. *Energ Fuel* 2015;29(1):413-27.
- 426 [20] Yue L, Xie HJ, Qin XM, Lu XX, Fang WJ. A DFT study on the thermal cracking of JP-10. *J*
427 *Mol Model* 2013;19(12):5355-65.
- 428 [21] Zehe MJ, Jaffe RL. Theoretical Calculation of Jet Fuel Thermochemistry. 1.
429 Tetrahydrodicyclopentadiene (JP10) Thermochemistry Using the CBS-QB3 and
430 G3(MP2)//B3LYP Methods. *J Org Chem* 2010;75(13):4387-91.
- 431 [22] Kuo KK, Risha GA, Evans BJ, Boyer E. Potential Usage of Energetic Nano-sized Powders
432 for Combustion and Rocket Propulsion. *MRS Proceedings* 2011;800.
- 433 [23] Yetter RA, Risha GA, Son SF. Metal particle combustion and nanotechnology. *P Combust*
434 *Inst* 2009;32:1819-38.
- 435 [24] Guo YS, Yang YZ, Xiao J, Fang WJ. A novel well-dispersed nano-Ni catalyst for
436 endothermic reaction of JP-10. *Fuel* 2014;117:932-8.
- 437 [25] E XTF, Zhang Y, Zou JJ, Wang L, Zhang XE. Oleylamine-Protected Metal (Pt, Pd)
438 Nanoparticles for Pseudohomogeneous Catalytic Cracking of JP-10 Jet Fuel. *Ind Eng Chem*
439 *Res* 2014;53(31):12312-8.
- 440 [26] Guo YS, Yang YZ, Fang WJ, Hu SL. Resorcinarene-encapsulated Ni-B nano-amorphous
441 alloys for quasi-homogeneous catalytic cracking of JP-10. *Appl Catal a-Gen* 2014;469:213-
442 20.
- 443 [27] Li D, Fang WJ, Wang HQ, Gao C, Zhang RY, Cai KK. Gold/Oil Nanofluids Stabilized by a
444 Gemini Surfactant and Their Catalytic Property. *Ind Eng Chem Res* 2013;52(24):8109-13.

- 445 [28] Wang JW, Liu Y, Zhang XW, Mi ZT, Wang L. Facile preparation of hydrocarbon fuel-
446 soluble nano-catalyst and its novel application in catalytic combustion of JP-10. *Catal*
447 *Commun* 2009;10(11):1518-22.
- 448 [29] Sabourin JL, Dabbs DM, Yetter RA, Dryer FL, Aksay IA. Functionalized Graphene Sheet
449 Colloids for Enhanced Fuel/Propellant Combustion. *ACS Nano* 2009;3(12):3945-54.
- 450 [30] Jain S, Park W, Chen YP, Qiao L. Flame speed enhancement of a nitrocellulose
451 monopropellant using graphene microstructures. *J Appl Phys* 2016;120(17).
- 452 [31] El-Seesy AI, Hassan H, Ookawar S. Performance, combustion, and emission characteristics
453 of a diesel engine fueled with Jatropha methyl ester and graphene oxide additives. *Energy*
454 *Convers Manage* 2018;166:674-86.
- 455 [32] Paramashivaiah BM, Banapurmath NR, Rajashekhar CR, Khandal SV. Studies on Effect of
456 Graphene Nanoparticles Addition in Different Levels with Simarouba Biodiesel and Diesel
457 Blends on Performance, Combustion and Emission Characteristics of CI Engine. *Arab J Sci*
458 *Eng* 2018;43(9):4793-801.
- 459 [33] Huang XF, Li SJ. Ignition and combustion characteristics of jet fuel liquid film containing
460 graphene powders at meso-scale. *Fuel* 2016;177:113-22.
- 461 [34] Ghamari M, Ratner A. Combustion characteristics of colloidal droplets of jet fuel and carbon
462 based nanoparticles. *Fuel* 2017;188:182-9.
- 463 [35] Li J-M, Chang P-H, Li L, Teo CJ, Khoo BC, Duan H, et al. Application of Graphene Oxide in
464 Jet A-1 in Air to Enhance Combustion Process. 2018 AIAA Aerospace Sciences Meeting.
465 American Institute of Aeronautics and Astronautics; 2018.
- 466 [36] Liu LM, Car R, Selloni A, Dabbs DM, Aksay IA, Yetter RA. Enhanced Thermal
467 Decomposition of Nitromethane on Functionalized Graphene Sheets: Ab Initio Molecular
468 Dynamics Simulations. *J Am Chem Soc* 2012;134(46):19011-6.

- 469 [37] Zhang CY, Wen YS, Xue XG. Self-Enhanced Catalytic Activities of Functionalized
470 Graphene Sheets in the Combustion of Nitromethane: Molecular Dynamic Simulations by
471 Molecular Reactive Force Field. *Acs Appl Mater Inter* 2014;6(15):12235-44.
- 472 [38] Senftle TP, Hong S, Islam MM, Kylasa SB, Zheng Y, Shin YK, et al. The ReaxFF reactive
473 force-field: development, applications and future directions. *npj Computational Materials*
474 2016;2:15011.
- 475 [39] Ashraf C, van Duin ACT. Extension of the ReaxFF Combustion Force Field toward Syngas
476 Combustion and Initial Oxidation Kinetics. *J Phys Chem A* 2017;121(5):1051-68.
- 477 [40] Chenoweth K, van Duin ACT, Goddard WA, 3rd. ReaxFF reactive force field for molecular
478 dynamics simulations of hydrocarbon oxidation. *J Phys Chem A* 2008;112(5):1040-53.
- 479 [41] Russo MF, van Duin ACT. Atomistic-scale simulations of chemical reactions: Bridging from
480 quantum chemistry to engineering. *Nucl Instrum Meth B* 2011;269(14):1549-54.
- 481 [42] van Duin ACT, Dasgupta S, Lorant F, Goddard WA. ReaxFF: A reactive force field for
482 hydrocarbons. *J Phys Chem A* 2001;105(41):9396-409.
- 483 [43] Feng M, Jiang XZ, Luo KH. A reactive molecular dynamics simulation study of methane
484 oxidation assisted by platinum/graphene-based catalysts. *P Combust Inst* 2018.
- 485 [44] Mao Q, van Duin ACT, Luo KH. Investigation of methane oxidation by palladium-based
486 catalyst via ReaxFF Molecular Dynamics simulation. *P Combust Inst* 2017;36(3):4339-46.
- 487 [45] Zhang YR, van Duin ACT, Luo KH. Investigation of ethanol oxidation over aluminum
488 nanoparticle using ReaxFF molecular dynamics simulation. *Fuel* 2018;234:94-100.
- 489 [46] Chenoweth K, van Duin ACT, Dasgupta S, Goddard WA. Initiation Mechanisms and
490 Kinetics of Pyrolysis and Combustion of JP-10 Hydrocarbon Jet Fuel. *J Phys Chem A*
491 2009;113(9):1740-6.
- 492 [47] Jiang XZ, Feng M, Zeng W, Luo KH. Study of mechanisms for electric field effects on
493 ethanol oxidation via reactive force field molecular dynamics. *P Combust Inst* 2018.

- 494 [48] Aktulga HM, Fogarty JC, Pandit SA, Grama AY. Parallel reactive molecular dynamics:
495 Numerical methods and algorithmic techniques. *Parallel Computing* 2012;38(4):245-59.
- 496 [49] Plimpton S. Fast Parallel Algorithms for Short-Range Molecular Dynamics. *Journal of*
497 *Computational Physics* 1995;117(1):1-19.
- 498 [50] Humphrey W, Dalke A, Schulten K. VMD: Visual molecular dynamics. *J Mol Graph Model*
499 1996;14(1):33-8.
- 500 [51] Henkelman G, Jonsson H. Improved tangent estimate in the nudged elastic band method for
501 finding minimum energy paths and saddle points. *J Chem Phys* 2000;113(22):9978-85.
- 502 [52] Henkelman G, Uberuaga BP, Jonsson H. A climbing image nudged elastic band method for
503 finding saddle points and minimum energy paths. *J Chem Phys* 2000;113(22):9901-4.
- 504 [53] Guo F, Cheng X, Zhang H. ReaxFF Molecular Dynamics Study of Initial Mechanism of JP-
505 10 Combustion. *Combust Sci Technol* 2012;184(9):1233-43.
- 506 [54] Davidson D, Horning D, Oehlschlaeger M, Hanson R. The decomposition products of JP-10.
507 37th Joint Propulsion Conference and Exhibit. American Institute of Aeronautics and
508 Astronautics; 2001.
- 509 [55] Wohlwend K, Maurice LQ, Edwards T, Striebich RC, Vangsness M, Hill AS. Thermal
510 stability of energetic hydrocarbon fuels for use in combined cycle engines. *J Propul Power*
511 2001;17(6):1258-62.

512